Journal of Nanoelectronics and Optoelectronics
Vol. 11, pp. 51–55, 2016
www.aspbs.com/jno

ARTICLE

Effect of an Electron Beam Treatment of the ZTO Active Layer on the Characteristics of Solution-Processed Thin-Film Transistors

Jae-Min Song[1], Byung Seong Bae[2], and Eui-Jung Yun[1,3,*]

This study examined the effects of the high-energy electron beam irradiation (HEEBI) of zinc-tin oxide (ZTO) on the device properties of TFTs with a sol–gel processed ZTO active layer. A higher negative-shifted threshold voltage ($-\Delta V_{th}$), lower field-effect mobility ($\mu_{sat\text{-}electron}$) and a higher resistivity of the active layer (ρ) were observed for the HEEBI-treated devices with a higher electron-beam dose. This suggests that a HEEBI-treatment with a higher dose causes an increase in the electron concentration in the ZTO due to the formation of oxygen vacancy donor defects, giving rise to a higher $-\Delta V_{th}$ and an increase in the barrier height at the drain/source and ZTO interfaces. This results in an increase in ρ, which in turn leads to a lower $\mu_{sat\text{-}electron}$. The effects of the HEEBI-treatment with a high dose on the device properties were stronger than those for the alloying step. The alloying step was more effective in improving the device properties of the solution-processed ZTO-TFTs than the HEEBI-treatment with a high dose. The experimental results are expected to contribute to the development of solution-processed ZTO TFTs with high performance and long-term reliability.

Keywords: Zinc Tin Oxide, Thin-Film Transistors, Solution-Processed, High-Energy Electron-Beam Irradiation (HEEBI).

1. INTRODUCTION

Recently, a few studies have shown that the optical and electrical properties of undoped ZnO films,[1–3] Al-doped ZnO films[4] and indium-Gallium ZnO (IGZO)-based thin film transistors (TFTs)[5] can be changed remarkably by a treatment with high-energy electron beam irradiation (HEEBI) at room temperature (RT). This suggests that studies of the variations in the properties in a radiation environment are gaining importance for the space applications of ZnO-based materials and devices.[1]

On the other hand, solution-processed ZTO thin films using spin coating,[6–10] dip coating,[11] or inkjet printing[12,13] have attracted considerable interest as the active layer in the fabrication of low-cost TFTs because of their chemical stability with respect to oxidation and etching, physical robustness, large area coverage, and high throughput.[6,7,9,14–19]

Until now, however, no attention has been devoted to a study of the device properties of solution- processed TFTs with ZTO treated by HEEBI at RT. Therefore, this study examined the effects of the HEEBI of ZTO on the device properties of TFTs with sol–gel processed ZTO.

2. EXPERIMENTAL DETAILS

The fabrication process of TFTs was as follows: The precursor solution for the ZTO active layer was synthesized using a sol–gel method by dissolving zinc acetate dihydrate and tin chloride powders in 2-methoxyethanol, which was stabilized with acetylacetone. The concentration of the precursor solution was 0.3 M with a Zn/Sn molar ratio of 1. The precursor solution was stirred for 8 hrs at 80 °C, filtered through a 0.2 μm membrane syringe filter and spin-coated at 4000 rpm for 50 sec on top of a 300-nm-thick SiO_2 gate dielectric layer grown thermally on a heavily-doped p-type Si gate electrode. A ZTO prebake process was then carried out at 100 °C for 1.5 min. on a hotplate

[1]Department of System Control Engineering, Hoseo University, Asan-City, Chungnam 336-795, Korea
[2]Department of Display Engineering, Hoseo University, Asan-City, Chungnam 336-795, Korea
[3]Department of Information and Communication Engineering, Hoseo University, Asan-City, Chungnam 336-795, Korea
*Author to whom correspondence should be addressed.
Email: ejyun@hoseo.edu
Received: 5 January 2015
Accepted: 18 March 2015

in air to evaporate the solvent. The precursor film was then converted to a 40-nm-thick ZTO active layer by annealing at 600 °C for 1 hr in a furnace. Some active layers were treated further with HEEBI in air at RT with an electron-beam energy of 0.8 MeV and doses ranging from 1×10^{14} to 1×10^{16} electrons/cm^2. To fabricate the TFTs, 100 nm Al source and drain electrodes were deposited through a shadow mask using a thermal evaporator. The alloying process was performed at 450 °C for 1 min. in N_2 with some TFTs to form Ohmic contacts between Al electrodes and a ZTO active layer. Here we emphasize that a short time of 1 min. was used for the alloying process in order to minimize the annealing effect on the ZTO-TFTs. Figure 1 shows the process flow for the fabrication of TFTs with a sol–gel processed ZTO active layer with or without the HEEBI treatment. Figure 1 illustrates the process flow used to fabricate the TFTs with the sol–gel processed ZTO active layer with or without the HEEBI treatment.

Figures 2(a) and (b) present a schematic cross-sectional view and a photographic top view, respectively, of a typical solution-deposited ZTO TFT developed in this study. As shown in Figure 2, the TFTs had a nonpatterned bottom gate and a top contact configuration. The channel width (W) and channel length (L) of the TFTs were 1500 μm and 100 μm, respectively.

The transfer and output characteristics of the developed ZTO-based TFTs were measured at RT in a darkened probe box in air using two Keithley 2400 source meters for a DC voltage source and a Keithley 6485 picoammeter for the current measurements. Two-terminal measurements involving the use of the source and drain electrodes were carried out after the TFTs had been placed on a darkened probe box.

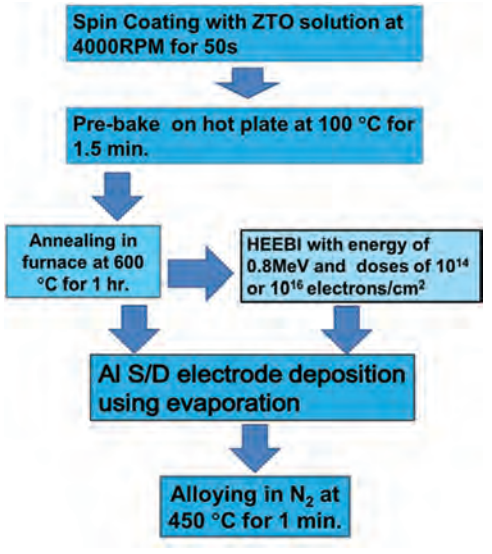

Fig. 1. Process flow for the fabrication of TFTs with sol–gel processed ZTO active layer with or without HEEBI treatment.

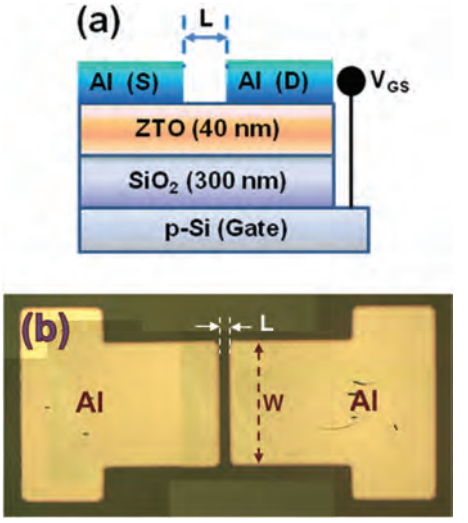

Fig. 2. (a) Schematic cross-sectional view and (b) photographic top view of the solution-processed ZTO-TFTs developed in this study: $W = 1500$ μm and $L = 100$ μm.

3. RESULTS AND DISCUSSION

Figure 3 shows the typical drain-to-source current versus gate-to-source voltage ($I_{DS} - V_{GS}$) transfer curves of TFTs with ZTO annealed at 600 °C and either untreated or treated with HEEBI, which were measured after the alloying process in N_2 at 450 °C for 1 min. All measurements were performed with the drain-to-source voltage (V_{DS}) fixed to 5 V, which is in the saturation region. The maximum I_{DS} in the saturation region ($I_{DS,sat}$) is given by the following equation:

$$I_{DS,sat} = \frac{W\mu_{sat\text{-}electron}C_{SiO_2}}{2L}(V_{GS} - V_{th})^2 \qquad (1)$$

where $\mu_{sat\text{-}electron}$ is the saturation-region electron field-effect mobility inside the n-type channel formed in the ZTO active layer, V_{th} is the threshold voltage and C_{SiO_2} is

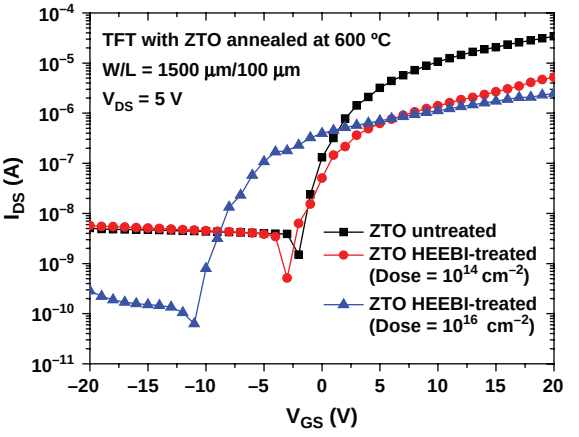

Fig. 3. I_{DS} versus V_{GS} transfer curve of the TFTs with ZTO annealed at 600 °C, untreated or treated with HEEBI, which were measured after alloying.

the capacitance per area of the SiO_2 gate insulator, which was 11.5 nF/cm^2, as measured in a metal-insulator-metal configuration. The $I_{DS}^{1/2}$ versus V_{GS} curves of the same TFTs used in Figure 3 (not shown) were obtained from the results in Figure 3 using Eq. (1). To estimate $\mu_{sat\text{-}electron}$, the slope of the linear portion of the $I_{DS}^{1/2}$ versus V_{GS} curves was substituted into Eq. (1). Therefore, if the device operates in saturation mode ($V_{DS} > V_{GS} - V_{th}$), $\mu_{sat\text{-}electron}$, in n-type operation, can be estimated from Ref. [19].

$$\mu_{sat\text{-}electron} = \left(\frac{\partial\sqrt{I_{DS}}}{\partial V_{GS}}\right)^2 \frac{2L}{W}\frac{1}{C_{SiO_2}} \quad (2)$$

The slope of the subthreshold swing (SS), which describes the change in V_{GS} that should be applied to the devices to increase I_{DS} by an order of magnitude, of the same devices used in Figure 3 was also obtained from the inverse slope of the curve in Figure 3 using Eq. (3)[20, 21]

$$SS = \left[\frac{d(\log I_{DS})}{dV_{GS}}\right]^{-1} \quad (3)$$

In the $I_{DS}^{1/2}$ versus V_{GS} curves, the extrapolation method[20] was also used to determine V_{th}. The resistivity of the active ZTO layer, ρ, was estimated using the following equation:[22]

$$\rho = \frac{Wt_{ZTO}}{I_{DS}L}V_{DS} \quad (4)$$

where t_{ZTO} is the thickness (40 nm) of the active ZTO layer.

Table I lists the important device parameters of the developed ZTO-TFTs, which were obtained from the results in Figure 3 using Eqs. (1)–(4). As shown in Figure 3 and Table I, the transfer curves of the all solution-processed TFTs with the ZTO active layers annealed and untreated with HEEBI showed good transfer characteristics and that a negative V_{GS} (a negative V_{th}) was required to deplete the electron carriers in the n-type active layer, which turned off the TFTs. This suggests that these TFT devices operate in depletion mode, exhibiting a normally on-channel state. For the TFTs with ZTO HEEBI-treated with a low dose of 10^{14} cm^{-2}, as shown in Figure 3 and Table I, a negative shift in $V_{th}(-\Delta V_{th} = 0.96$ V) and an increase in SS were observed. An increase in SS would be related to an increase in the density of the subgap trap states at the Fermi level (E_F), which are located close to the semiconductor/insulator interfaces.[23] Therefore, the $-\Delta V_{th}$ shift, which is accompanied by an increase in SS, is believed to be due to an increase in the number of hole trap states in the ZTO active layer or at the ZTO/insulator interface due to the HEEBI treatment at a low dose. As a result, the electron concentration in the ZTO active layer increased, resulting in a $-\Delta V_{th}$ shift. Table I also shows that the HEEBI treatment with a low dose causes a decrease in both the $I_{on/off}$ and the $\mu_{sat\text{-}electron}$ because the ρ values at the on-state ($V_{GS} = 20$ V) increase with increasing dose while those at the off-state ($V_{GS} < 0$ V) remain unchanged. The increase in ρ at the on state will induce a decrease in I_{DS} at the on-state, which leads to a decrease in $I_{on/off}$. An increase in ρ in the active layer results in a decrease in $\mu_{sat\text{-}electron}$ based on the equation, $\mu_{sat\text{-}electron} = 1/(nq\rho)$, where q is the charge of an electron and n is the electron carrier concentration.

In the case of TFTs with ZTO HEEBI-treated with a high dose of 10^{16} cm^{-2}, Figure 3 and Table I revealed a severer negative shift of $V_{th}(-\Delta V_{th} = 6.11$ V), a decrease in SS, a further decrease in $\mu_{sat\text{-}electron}$, a further increase in ρ, and an increase in $I_{on/off}$ compared to those parameters for the low dose case. Here, a decrease in SS can be attributed to a decrease in the number of hole trap states in ZTO and/or at the ZTO/SiO_2 interfaces[23, 24] because of the annealing effect of high-energy electrons irradiated on the ZTO produced by particle radiation-matter interaction. This decrease in SS caused by the annealing effect of the high dose HEEBI treatment can enhance both the barrier height for hole injection at the drain/ZTO interface (ΔE_V) and that for electron injection at the source/ZTO interface (ΔE_C), resulting in decreases in both the off and on I_{DS} currents, which in turn leads to an increase in ρ in the active layer. These results agree well with the data shown in Figure 3 and Table I.

Table I. Summary of the important device parameters of the developed ZTO-TFTs, which were obtained from the results shown in Figure 3 using Eqs. (1)–(4).

Sample description	$I_{on/off}^{(a)}$	$SS^{(b)}$ (V/dec.)	$V_{th}^{(c)}$ (V)	$\mu_{sat\text{-}electron}^{(d)}$ (cm^2/Vs)	$\rho^{(e)}$ at $V_{GS} = 20$ V (Ωcm)	$\rho^{(f)}$ at $V_{GS} < 0$ V (Ωcm)
TFTs with ZTO annealed and untreated by HEEBI (S1)	0.9×10^4	1.16	−1.02	1.17	8.8	7.4×10^4
TFTs with ZTO annealed and treated by HEEBI with dose of 10^{14} cm^{-2} (S2)	1.5×10^3	2.13	−1.98	0.18	57.7	7.4×10^4
TFTs with ZTO annealed and treated by HEEBI with dose of 10^{16} cm^{-2} (S3)	1.8×10^4	1.72	−8.09	0.06	120.5	2.1×10^6

Notes: [a]On–off ratio for drain current, [b]Sub-threshold swing obtained from Eq. (3), [c]Threshold voltage obtained from Eq. (1), [d]Saturation-region electron field-effect mobility obtained from Eq. (2), [e]On-state resistivity at $V_{GS} = 20$ V obtained from Eq. (4), [f]Off-state resistivity at $V_{GS} < 0$ V obtained from Eq. (4).

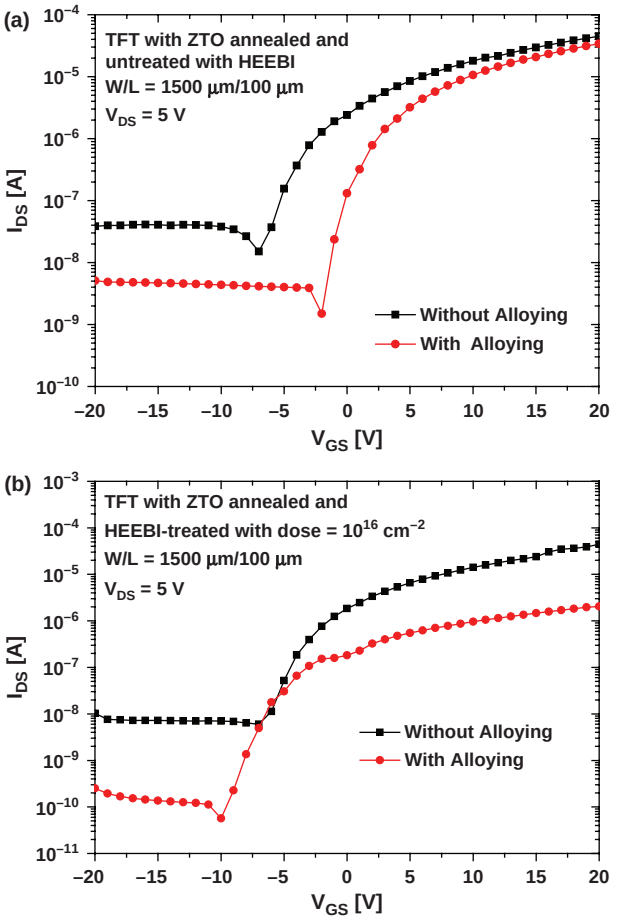

Fig. 4. Typical $I_{DS} - V_{GS}$ transfer characteristics of the TFTs with ZTO annealed at 600 °C as well as (a) untreated and (b) treated by HEEBI at a dose of 1×10^{16} electrons/cm^2 at a fixed V_{DS} of 5 V, which were measured before and after the alloying step in N_2 at 450 °C for 1 min.

The huge $-\Delta V_{th}$ with a high dose of HEEBI treatment was attributed to an increase in the electron carrier concentration (n) in the ZTO due to formation of oxygen vacancy donor defects with the HEEBI treatment of ZTO. This leads to an increase in ρ in the ZTO active layer, giving rise to a decrease in $\mu_{sat\text{-}electron}$ via the relation $\mu_{sat\text{-}electron} = 1/(nq\rho)$, as evident in Figure 3 and Table I. Table I also shows that the increase in ρ in the active layer at the off-state is considerably more severe than that at the on-states, causing an increase in the $I_{on/off}$ for the case of the HEEBI-treatment with a high dose.

Figure 4(a) shows the typical $I_{DS} - V_{GS}$ transfer characteristics of TFTs with ZTO annealed at 600 °C and untreated by HEEBI at a fixed V_{DS} of 5 V, which were measured before and after the alloying step in N_2 at 450 °C for 1 min. Figure 4(b) also shows the typical $I_{DS} - V_{GS}$ transfer characteristics of the TFTs with ZTO annealed at 600 °C and treated by HEEBI at a dose of 1×10^{16} electrons/cm^2 at a fixed V_{DS} of 5 V, which were measured before and after the alloying step in N_2 at 450 °C for 1 min. Table II summarizes the important device parameters of the ZTO-TFTs untreated and treated by HEEBI at a high dose of 1×10^{16} electrons/cm^2 using Eqs. (1)–(4), which were obtained from the results in Figures 4(a) and (b), respectively. As shown in Figure 4(a) and Table II, for the samples untreated by HEEBI, a positive shift of V_{th} ($\Delta V_{th} = 5.46$ V), a decrease in SS, a slight increase in $\mu_{sat\text{-}electron}$, a large increase in ρ at the off-state compared to a small increase in ρ at on-state, and an increase in $I_{on/off}$ were observed after the alloying step in N_2 at 450 °C for 1 min. This suggests that the alloying step is useful for developing solution-processed ZTO-TFTs with high performance. A decrease in SS can also be related to a decrease in the number of hole trap states in ZTO and/or at the ZTO/SiO_2 interface,[23, 24] which is similar to the annealing effect observed in the case of the HEEBI treatment with a high dose. This decrease in SS caused by the alloying process can cause an increase in both ΔE_V and ΔE_C, resulting in decreases in the off I_{DS} current, which in turn leads to an increase in ρ at the off-state. These results agree well with the observations shown in Figure 4(a) and Table II. A huge positive shift of V_{th} with

Table II. Summary of the important device parameters of the developed ZTO-TFTs, which were obtained from the results in Figure 4 using Eqs. (1)–(4).

Sample description	$I_{on/off}$	SS (V/dec.)	V_{th} (V)	$\mu_{sat\text{-}electron}$ (cm^2/Vs)	ρ at $V_{GS} = 20$ V (Ωcm)	ρ at $V_{GS} < 0$ V (Ωcm)
TFTs with ZTO annealed and untreated by HEEBI, without alloying (S4)	1.3×10^3	2.82	−6.48	0.77	6.7	7.4×10^3
TFTs with ZTO annealed and untreated by HEEBI, with alloying (S1)	0.9×10^4	1.16	−1.02	1.17	8.8	7.4×10^4
TFTs with ZTO annealed and treated by HEEBI with dose of 10^{16} cm^{-2}, without alloying (S5)	6.5×10^3	1.70	−5.97	0.74	6.7	4.3×10^4
TFTs with ZTO annealed and treated by HEEBI with dose of 10^{16} cm^{-2}, with alloying (S3)	1.8×10^4	1.72	−8.09	0.06	120.5	2.2×10^6

an alloying treatment is due likely to a decrease in the electron carrier concentration (n) in the ZTO because of a decrease in the number of oxygen vacancy donor defects with an alloying step, which causes an increase in the off-state ρ in the ZTO active layer. This increase in ρ and the decrease in n lead to a slight increase in $\mu_{\text{sat-electron}}$. The increase in ρ at the off-state and the almost unchanged ρ at the on-states also causes an increase in $I_{\text{on/off}}$ in the case of the alloy-treatment.

On the other hand, the samples treated by HEEBI with a dose of 1×10^{16} electrons/cm^2 exhibited a negative shift of $V_{\text{th}}(-\Delta V_{\text{th}} = 2.12$ V), slight increases in SS and $I_{\text{on/off}}$, a decrease in $\mu_{\text{sat-electron}}$, and large increases in ρ at both the off- and on-states after the alloying step, as shown in Figure 4(b) and Table II, which are similar to the device properties observed in the case of the HEEBI-treatment with a high dose. This suggests that the effects of the HEEBI-treatment with a high dose on the device properties are stronger than those for an alloying step. Based on the results shown in Figure 4 and Table II, it was concluded that the alloying step was more effective in producing solution-processed ZTO-TFTs with high performance than the HEEBI-treatment with a high dose.

4. CONCLUSION

This study examined the effects of the HEEBI of ZTO on the device properties of TFTs with a sol–gel processed ZTO active layer. For the TFTs with ZTO HEEBI-treated with a low dose of 10^{14} cm^{-2}, the $-\Delta V_{\text{th}}$ shift, which is accompanied by an increase in SS, was attributed to an increase in the electron concentration in the ZTO caused by an increase in the number of trap states in the ZTO or at the ZTO/insulator interface due to the HEEBI treatment. The HEEBI treatment with a low dose also caused decreases in both the $I_{\text{on/off}}$ and $\mu_{\text{sat-electron}}$, which can be attributed to the on-state ρ values increasing with increasing dose while those at the off-state remain unchanged. On the other hand, in the case of the TFTs with ZTO HEEBI-treated with a high dose of 10^{16} cm^{-2}, the decrease in SS caused by the annealing effect of the HEEBI treatment with a high dose can enhance both the ΔE_V and ΔE_C, resulting in an increase in ρ in the active layer. A huge $-\Delta V_{\text{th}}$ with a high dose of the HEEBI treatment is due likely to an increase in the electron concentration in ZTO due to the formation of oxygen vacancy donor defects with the HEEBI treatment. This leads to an increase in ρ in the ZTO active layer and a decrease in $\mu_{\text{sat-electron}}$ via the relation, $\mu_{\text{sat-electron}} = 1/\text{nq}\rho$. The increase in the off-state ρ is much higher than that at the on-states, causing an increase in the $I_{\text{on/off}}$ in the case of the HEEBI-treatment with a high dose. The alloying step was more effective in developing solution-processed ZTO-TFTs with high performance than the HEEBI-treatment with a high dose.

Acknowledgments: This study was supported by the Academic Research Fund of Hoseo University in 2014 (FRC-2014-0082).

References and Notes

1. E. Gür, H. Asil, C. Coşkun, S. Tüzemen, K. Meral, Y. Onganer, and K. Şerifoğlu, *Nucl. Instrum. Meth. Phys. Res. B* 266, 2021 **(2008)**.
2. E.-J. Yun, J. W. Jung, Y. H. Han, M.-W. Kim, and B. C. Lee, *J. Appl. Phys.* 105, 123509 **(2009)**.
3. E.-J. Yun, J. W. Jung, Y. H. Han, M.-W. Kim, and B. C. Lee, *J. Korean Phys. Soc.* 56, 356 **(2010)**.
4. E.-J. Yun, J. W. Jung, and B. C. Lee, *J. Alloys Compd.* 496, 543 **(2010)**.
5. H. J. Moon, H. R. Oh, B. S. Bae, M. K. Ryu, K. I. Cho, and E.-J. Yun, *J. Korean Phys. Soc.* 60, 187 **(2012)**.
6. Y. B. Yoo, J. H. Park, S. J. Lee, K. M. Song, and H. K. Baik, *Jpn. J. Appl. Phys.* 51, 040201 **(2012)**.
7. C. G. Lee, B. Cobb, and A. Dodabalapur, *Appl. Phys. Lett.* 97, 203505 **(2010)**.
8. C. G. Lee and A. Dodabalapur, *J. Electron. Mater.* 41, 895 **(2012)**.
9. Y. H. Hwang, S.-J. Seo, J.-H. Jeon, and B.-S. Bae, *Electrochem. Solid-State Lett.* 15, H91 **(2012)**.
10. W. Hu and R. L. Peterson, *J. Mater. Res.* 27, 2287 **(2012)**.
11. B. N. Pal, B. M. Dhar, K. C. See, and H. E. Katz, *Nature Mater.* 8, 898 **(2009)**.
12. Y. H. Kim, K. H. Kim, M. S. Oh, H. J. Kim, J. I. Han, M. K. Han, and S. K. Park, *IEEE Electron Device Lett.* 31, 836 **(2010)**.
13. D. Kim, Y. Jeong, K. Song, S. K. Park, G. Cao, and J. Moon, *Langmuir* 25, 11149 **(2009)**.
14. S. Jeong, Y. Jeong, and J. Moon, *J. Phys. Chem. C* 112, 11083 **(2008)**.
15. C.-G. Lee and A. Dodabalapur, *Appl. Phys. Lett.* 96, 243501 **(2010)**.
16. Y. H. Hwang, S.-J. Seo, J.-H. Jeon, and B.-S. Bae, *Electrochem. Solid-State Lett.* 15, H91 **(2012)**.
17. C. G. Kim, N.-H. Lee, Y.-K. Kwon, and B. Kang, *Thin Solid Films* 544, 129 **(2013)**.
18. H. B. Kim and H. S. Lee, *Thin Solid Films* 550, 504 **(2014)**.
19. L. Schulz, E.-J. Yun, and A. Dodabalapur, *Appl. Phys. A* 115, 1103 **(2014)**.
20. D. C. Paine, B. Yaglioglu, Z. Beiley, and S. Lee, *Thin Solid Films* 516, 5894 **(2008)**.
21. K. M. Yu, J. T. Yuh, S. H. K. Park, M. K. Ryu, E. J. Yun, and B. S. Bae, *Jpn. J. Appl. Phys.* 52, 10MA12 **(2013)**.
22. J. H. Chung, J. Y. Lee, H. S. Kim, N. W. Jang, and J. H. Kim, *Thin Solid Films* 516, 5597 **(2008)**.
23. T. Kamiya and H. Hosono, *NPG Asia Mater.* 2, 15 **(2010)**.
24. J. T. Yuh and B. S. Bae, *Electron. Mater. Lett.* 6, 22106 **(2010)**.